European Polymer Journal 44 (2008) 2790–2797

Contents lists available at ScienceDirect

European Polymer Journal

journal homepage: www.elsevier.com/locate/europolj

Macromolecular Nanotechnology

Physical properties of silicone foams filled with carbon nanotubes and functionalized graphene sheets

Raquel Verdejo [a,*], Cristina Saiz-Arroyo [b], Javier Carretero-Gonzalez [a], Fabienne Barroso-Bujans [a], Miguel Angel Rodriguez-Perez [b], Miguel Angel Lopez-Manchado [a,*]

[a] Institute of Polymer Science and Technology (CSIC), Juan de la Cierva, 3, Madrid 28006, Spain
[b] Cellular Materials Group (CellMat), Condensed Matter Physics Department, University of Valladolid, Valladolid 47011, Spain

ARTICLE INFO

Article history:
Received 11 June 2008
Received in revised form 19 June 2008
Accepted 24 June 2008
Available online 1 July 2008

Keywords:
Functionalized graphene sheets
Carbon nanotubes
Foams
Silicone

ABSTRACT

Free-rising silicone foams were made with loading fractions of up to 0.25 wt.-% functionalized graphene sheets (FGS) and up to 1.0 wt.-% carbon nanotubes (CNTs) using hydrogen as blowing agent. Scanning electron microscopy of the samples revealed an open cellular structure and a homogeneous dispersion of both types of nanofillers. The incorporation of nanofiller affected the foaming process and thus the final foam density and cellular structure. Transmission electron microscopy revealed the formation of a CNT network throughout the sample, while FGS presented an exfoliated and intercalated dispersion. The thermal stability of the samples was drastically affected by the presence of both nanofillers. Both nanofillers showed a positive effect on the compressive response of the foams. However, the nanocomposite foams were found to decrease the acoustic absorption with nanofiller content probably due to the variable foam structure and improved stiffness.

Introduction

The addition of carbon nanotubes (CNTs) to polymer matrices has already been shown to improve their mechanical, electrical and thermal properties [1,2]. However, progress has been partly limited by the availability of high-quality nanomaterials, price and by fundamental composite issues relating to dispersion, alignment, and interfacial adhesion. Hence, a successful approach was to reinforce delicate systems where conventional fibres cannot be physically accommodated, such as films [3–8], fibres [8–10] and foams [11–17]. Lately, the challenge has been to exfoliate the graphite to single graphene sheets [18–20] to use it as an inexpensive and feasible substitute to CNTs. The predicted properties of this type of nanofillers suggest a number of applications on mechanical, electrical and chemical engineering processes [21]. Previous attempts to produce graphite nanolayers used expanded graphite, which is made from the rapid thermal expansion of sulphuric acid-intercalated graphite [22–28]. However, none of these materials achieved the complete exfoliation of graphite in its individual graphene sheets as evidenced by the presence of graphite diffraction peaks in the XRD patterns [23,26,27]. Recently, it has been suggested that the starting material to achieve single graphene sheets is graphite oxide (GO). The GO is made by the oxidation of natural graphite and gives way to functionalized graphene sheets (FGS) [19] through an adequately thermal expansion, or to single graphene sheets [20] through the chemical reduction of exfoliated GO. Successful examples of graphene-based or FGS-based nanocomposites have recently been reported [29–31].

The aim of the present study was to investigate the effects of two types of carbon-based nanofillers, in particular CNTs and FGS, on the cellular structure, morphology, and properties of silicone foams. These carbon nanostructures, with their high mechanical properties and high aspect ratios, have particular potential to modify both the

* Corresponding authors.
E-mail addresses: rverdejo@ictp.csic.es (R. Verdejo), lmanchado@ictp.csic.es (M.A. Lopez-Manchado).

0014-3057/$ - see front matter © 2008 Elsevier Ltd. All rights reserved.
doi:10.1016/j.eurpolymj.2008.06.033

foaming processes and to enhance the physical performance of the final cellular composite. Here, we provide a detailed analysis of the properties of the foam products and the effects on the foam microstructures.

Polymeric foams are important and versatile materials due to their outstanding strength to weight ratio, their resilience, and their electrical, thermal, and acoustic insulation properties, among other characteristics. The selection of the appropriate reactants and manufacturing technology enables the production of a particular foam to satisfy the wide-range of applications [32].

Free-rise silicone foams are generally obtained from the simultaneous reaction of silanols (SiOH) on hydroxyl-terminated polydimethylsiloxane and silanes (SiH) on polymethylhydrogensilane in presence of a catalyst. This reaction generates hydrogen which drives the foam expansion. Meanwhile, the crosslinking takes place by the addition-cure reaction of vinyl endblocked groups with Si–H groups [33].

Experimental details

Materials and sample preparation

The vapour-grown CNTs were supplied by Bayer, Germany (Baytubes® C 150 P). The as-received MWCNTs have a mean diameter of 13.5 ± 6.4 nm and is free of carbonaceous contaminations. Graphite oxide was produced using natural graphite powder (universal grade, 200-mesh, 99.9995%) according to the Brodie method [30,34].

Commercially available silicone foam reactants were kindly supplied by Bluestar Silicones (Rhodorsil RTFoam 3240) without any commercial filler. The system was composed of two reactants: a polymethylhydrogensilane (≡SiH) and a hydroxyl-terminated polydimethylsiloxane (≡SiOH) compound containing the Pt catalyst.

Both CNTs and FGS were dispersed in ethanol (10 ml) for 5 min using an ultrasonication probe and left stirring overnight. This mixture was subsequently dispersed under high shear mixing in the ≡SiH compound, to prevent inhibition of the Pt catalyst. Meanwhile, the ethanol was evaporated until a constant weight was achieved. Finally, the ≡SiOH compound was thoroughly mixed with the CNT/≡SiH compound at a 1:1 ratio for 15s. The final mixture was poured into a rectangular mould and foaming occurred. Foams containing 0.10, 0.50 and 1.00 wt.-% CNTs and 0.10, 0.20 and 0.25 wt.-% FGS were produced.

Sample characterisation

The porous structure was qualitatively examined using a Philips XL30 scanning electron microscope (FEGSEM) at 15 kV, after sputter-coating with platinum-gold. Cross-sections of the foams were cryo-fractured perpendicular to the foaming direction. Images were analysed using Image J software (W.S. Rasband, US. National Institutes of Health, Bethesda, MD, USA, www.rsb.info.nih.gov/ij/), taking Feret's diameter as a measure of average cell size. Prior to the analysis, the pores were traced manually and a grey-scale image was obtained by scanning the outlined structure. Mean cell size was an average value obtained from measuring three different regions with a minimum of 200 cells per foam.

TEM images were obtained with a Philips Tecnai 20 TEM apparatus using an accelerating voltage of 200 kV. The samples were 40–50 nm thick and were prepared with a LEICA EM UC6 ultracryomicrotome, cutting at −140 °C.

The polymer matrix density (ρ_m) was obtained from 10 cubic samples which were cut from different areas of the sample using helium displacement pycnometry (Micromeritics AccuPyc 1330) and analysed to obtain statistically relevant data. Foam density (ρ_f) was measured using a hydrostatic balance (Kern Densimeter) applying the Archimedes' principle:

$$\rho_f = \frac{w_1}{w_1 - w_2}\rho_w + \rho_g$$

where w_1 is the weight of the sample in air, w_2 is its weight immersed in water, ρ_w is the water density and ρ_g (0.00129 g/cm^3) is the air density at standard pressure and temperature.

Thermo-gravimetric analysis (TGA) was carried out on Q500 from TA instruments. The sample was placed on a platinum holder and heated to 850 °C, at a heating rate of 10 °C min^{-1}, under a nitrogen flow of 100 ml min^{-1} to prevent carbon oxidation.

Creep experiments were measured using Perkin Elmer 7 at room temperature. Rectangular foam pieces, 7.6 ± 0.2 mm in height, 9.2 ± 0.1 mm width and 9.2 ± 0.1 mm depth, were compressed at 150 mN/min loading rate until the loading head reached its limit. The results were an average value obtained from measuring at least three different foam samples.

Small scale acoustic testing was performed according to ASTM E150 and ISO 10534-2 using a Brüel & Kjær acoustic test system comprising of an impedance tube, two microphones and a digital frequency analyser. The absorption coefficient (α) was calculated as the average value of two cylindrical foam pieces, 30 mm diameter and 10 mm thickness over the frequency range from 500 to 6400 Hz. Each sample was measured twice on both sides. The normalized absorption coefficient, also known as acoustic activity, was calculated according to:

$$\alpha_n = \frac{\int_{f_1}^{f_2} \alpha(f)\mathrm{d}f}{f_2 - f_1}$$

where f_1 is the lower frequency limit, 500 Hz, and f_2 the upper frequency limit, 6400 Hz.

Results and discussion

Adding both nanofillers into the ≡SiH compound noticeably increased the viscosity of the mixture, and reached a tar-like consistency at 0.3 wt.-% FGS and 1.2 wt.-% CNT. Due to this viscosity increase, the system no longer foamed properly. This increase in the mixture viscosity would have affected the foaming process, as the evolution of the blowing agent (in this case H_2) is influenced by the rheological properties of the polymer and the kinetics of the reaction [35]. Although the eventual

volume of the foam was restricted, the rising time was extended in comparison with that of the control system. This lower foaming rate would have affected the cellular structure of the foams, promoting gas diffusion from small cells to larger ones in order to reduce both the increment in free energy within the system and the pressure difference between the gas and the surrounding liquid [35]. The smaller volume of the nanocomposite samples could also have been due to the nanofillers acting as additional crosslink points and affecting the gelation or polymerisation of the cellular structure, thereby causing a higher density. Furthermore, the gelation of the filled samples was qualitatively slower. The combination of these effects hence suggested a slower reaction rate of the nanocomposite foams than that of the control sample.

SEM imaging (Fig. 1) and image analysis (Fig. 2) confirmed the changes in the cellular structure of both types of nanocomposite foams. The unfilled silicone foam had an isotropic structure of relatively spherical cells with interconnected pores, while the filled samples exhibited a reduction in both cell roundness and cell connectivity, with adjacent cells seem to have coalesced. Additionally, filled samples exhibited thicker cell walls than those of the control that affected the final density of the samples (as discussed below). In contrast with previous results reported for nanocomposite foams, which showed a reduction in cell size due to high viscosity and nucleating effects [36,37], we observed the opposite tendency (Table 1). This difference was attributed to the foaming process. Cell size in reacting foams depends on the reaction rate, which determines both the production of gas and the evolution of the fluid rheology, coupled to the rate of gas diffusion [38]. Everitt et al. [38] modelled bubble dynamics for reacting foams and showed that, at low reaction rates, the final bubble volume is independent of diffusivity and reaches its equilibrium size before gelation takes place. Hence, the current trends in cell size were more probably related to the production of gas and the evolution of the fluid rheology. An additional factor to be considered is a probable reduction in the pore nucleation rate due to the given logarithmic proportionality between viscosity and surface tension for many fluids [32], including polymers, and the known influence of CNTs on viscosity [39]. In the current study, there was no evidence of any nucleation effects due to the presence of the nanofillers [37] which ought to lead to smaller cell sizes even at low loading fractions.

Numerical simulations have suggested a substantial contribution of nanoparticle shape in the rheology of polymer nanocomposites [40]. Hence, cell size distributions (Fig. 2) were examined to reveal differences of the nanofillers effect on the cellular structure. It can be observed that the normal distribution becomes wider with the addition of both nanofillers. However, filler shape did not seem to affect the mean cell size distribution of the samples. Cell size distributions of the samples with similar loading

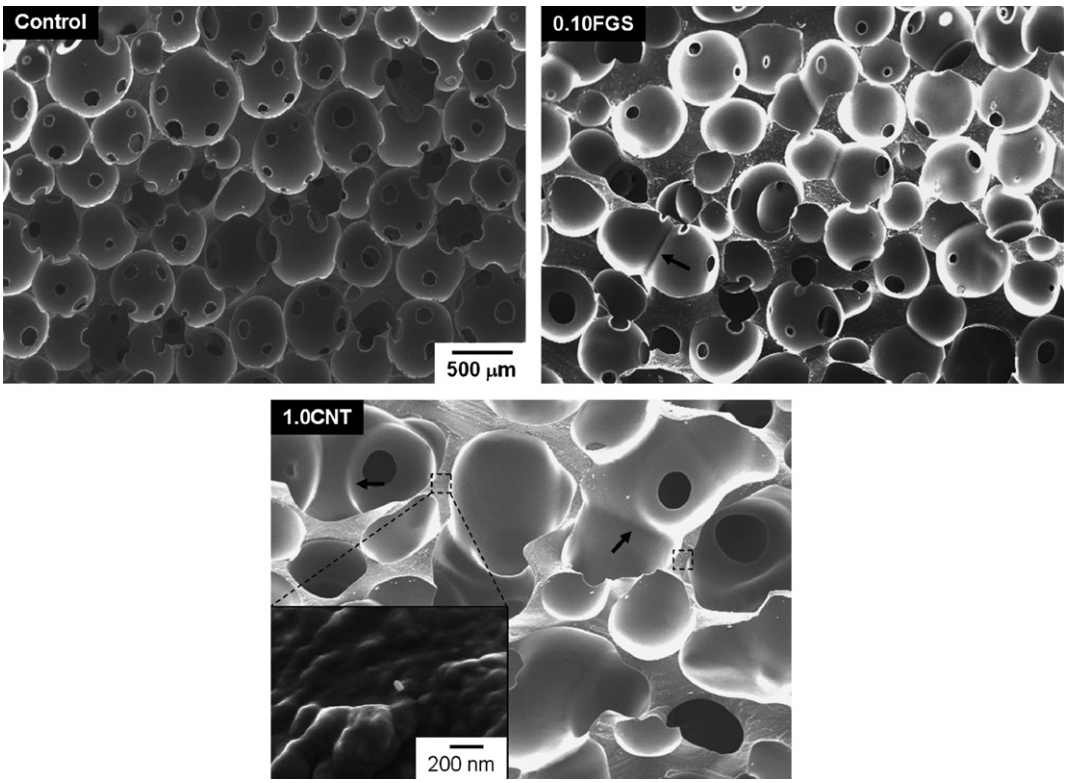

Fig. 1. Representative SEM images of nanocomposite foams at low and high loading fractions. Arrows indicate merged cells. The insert SEM micrograph in 1.0 wt.-% CNT sample showed a CNT emerging from the cell surface.

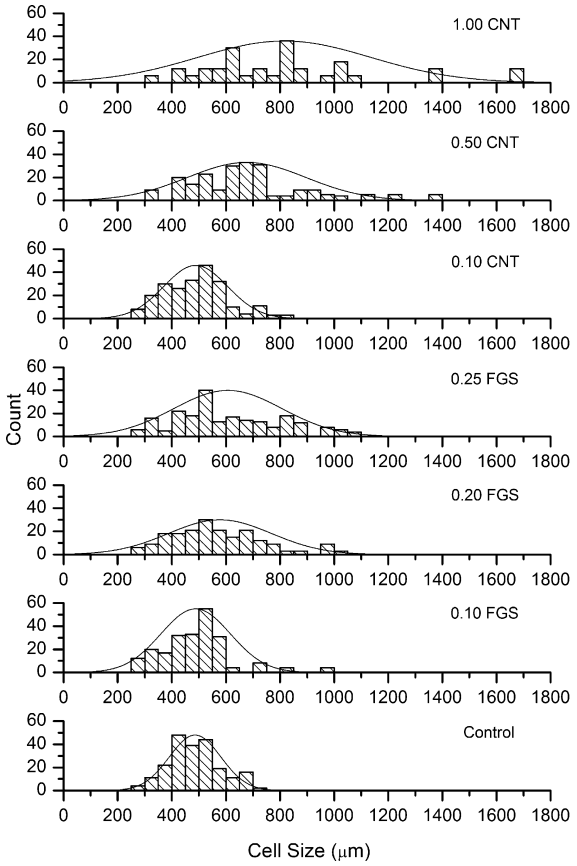

Fig. 2. Cell size distributions as a function of the nanofiller content of the silicone foams.

fraction appeared both very similar, with a slight shift towards lower cell sizes of the CNT sample.

The dispersion of the nanofillers was investigated by TEM. The exfoliation process of the functionalized graphene sheets has been observed to produce a defective wrinkle structure with large surface area 700–1500 m^2/g [19]. TEM micrographs of the FGS layers [30] showed almost transparent sheets with the wrinkle structure and the presence of stacks of a limited number of graphene sheets with inter-layer spacing of 0.6 nm. The FGS morphology suggested that the nature of the dispersion would be composed of both exfoliated and intercalated, which is common in nanocomposites containing layered fillers [41]. TEM observation confirmed this dual dispersion, as the FGS were distributed over the entire sample and the particles appeared to be completely embedded in the polymer matrix indicating the intercalated structure (Fig. 3a). This homogeneous dispersion would probably be related to the presence of remaining oxygen-containing groups on the graphite sheets. These groups have been associated to isolated epoxy and hydroxyl reaction sites [19]. The presence of the hydroxyl groups can be expected to covalently bond to the SiH-containing component of the reaction mixture during curing.

The CNT/silicone samples revealed an unexpected CNT morphology. The CNTs formed a network throughout the sample (Fig. 3b). The probable mechanism responsible for the dispersion of these CNTs was the presence of CH–π interactions, as the nature of the rubber matrix would have prevented it from forming π–π interactions with CNTs. CH-π interactions are a type of hydrogen bond that operates between a soft acid CH and a soft base π-system, as found on the convex surfaces of fullerenes and nanotubes [42]. The dispersion of carbonaceous materials, such as carbon blacks and carbon fibres, in rubber matrices has also been linked to CH–π interactions [43].

Table 1 shows the foam and polymer densities. The density of the polymer matrix increased with nanofiller content, as expected, since the graphitic material is denser than the matrix polymer. The increase in the foam densities was attributed to the observed changes in the cellular structure, because it cannot be completely attributed to the higher intrinsic density of the nanofillers.

Fig. 4 shows the evolution of the weight loss as a function of the temperature of the control matrix and low loading fractions under nitrogen atmosphere. The control sample exhibited a sharp weight loss centred at 468 °C, which corresponds to the depolymerisation of the siloxane chains [44]. Meanwhile, the weight loss of the filled samples was less pronounced and showed a clear shift in both the onset temperature and the main degradation temperature (T_{peak}) towards higher temperatures. Furthermore, the filled formulations showed a significant increase in total residue (Table 2) at 650–700 °C. Hence, both nanofillers significantly improved the thermal stability of the samples. This improvement in thermal stability had previously been observed in nanotube composites based on other polymers, and various mechanisms have been suggested to explain it [45]: (1) dispersed nanotubes may hinder the flux of degradation product, delaying the onset of degradation; (2) polymer chains near the nanotubes may degrade more slowly, shifting T_{peak} to higher temperatures; (3) higher thermal conductivity in the nanotube/polymer composites

Table 1
Mean cell size and measured densities and relative density of the samples

Samples wt.-%	Mean cell size (μm)	Foam density (ρ_f) (kg/m^3)	Polymer density (ρ_m) (kg/m^3)	Relative density (%) (ρ_f/ρ_m)
0	486 ± 6	197 ± 17	1078 ± 2	18.3
0.10 FGS	488 ± 9	278 ± 11	1080 ± 5	25.7
0.20 FGS	608 ± 13	282 ± 8	1081 ± 1	26.1
0.25 FGS	578 ± 13	291 ± 9	1082 ± 3	26.9
0.10 CNT	489 ± 8	258 ± 18	1081 ± 2	23.8
0.50 CNT	677 ± 15	272 ± 10	1082 ± 3	25.2
1.00 CNT	816 ± 22	291 ± 19	1084 ± 4	26.9

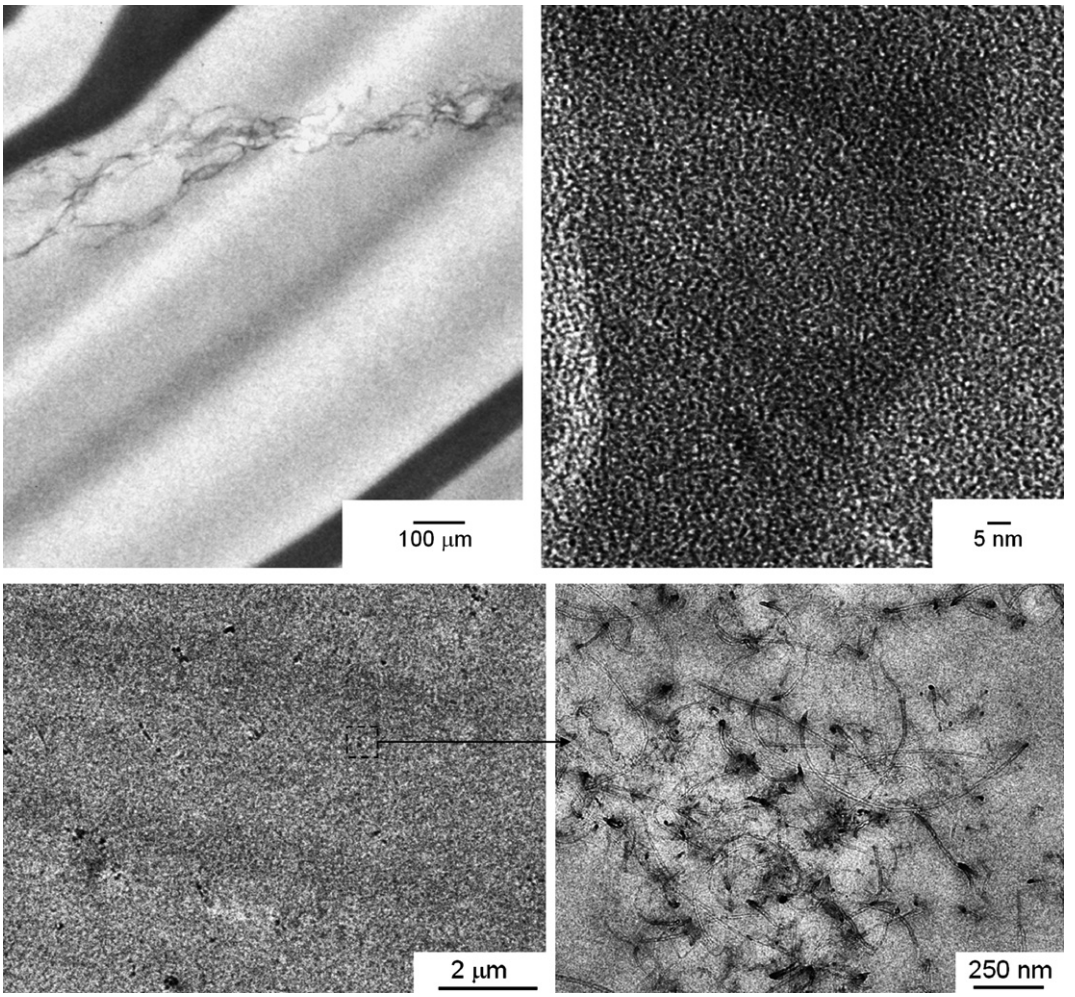

Fig. 3. TEM images of the nanocomposite samples. (a) 0.25 wt.-% FGS, the dark lines of the image correspond to folds of the matrix, and (b) 1.0 wt.-% CNT filled silicone foams.

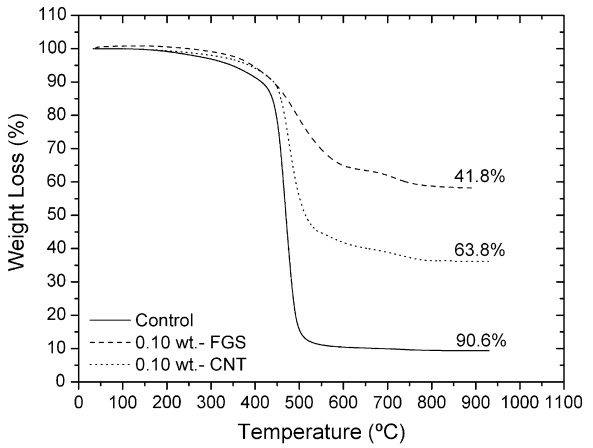

Fig. 4. Representative weight loss as a function of temperature.

could ease heat dissipation within the composite. The thermal degradation of filled samples showed a second step at higher temperatures (720–740 °C), which was probably due to an increase in the rigidity of the siloxane chains [46]. Previous results on silicone samples filled with carbon black showed a change to multistage degradation [46].

Table 2
Thermogravimetric results of the samples

Samples wt.-%	T_{peak} (°C)	T_2 (°C)	Weight loss (%)
0	468	–	90.6
0.10 FGS	516	734	41.8
0.20 FGS	522	746	37.6
0.25 FGS	524	744	36.1
0.10 CNT	475	721	63.8
0.50 CNT	518	725	53.8
1.00 CNT	523	728	48.0

The T_{peak} (Table 2) increased as a function of nanofiller content by up to 55 °C. Graphene sheets were more effective than nanotubes to improve the thermal stability of the silicone foams, as the same degradation temperature was obtained at much lower filler content. Furthermore,

at the same filler loading, FGS filled silicone foams exhibited higher T_{peak} than that of CNT filled samples. This difference was attributed to an increased confinement of the polymer matrix in the intercalated structure, also observed in nanoclay/polydimethylsiloxane systems [47], and to stronger polymer/graphene interactions.

Compressive results of the nanocomposite foams are shown in Fig. 5. The control sample exhibited the typical compressive behaviour of foams, while both FGS and CNT samples just exceeded the yield point or showed only the linear region just before the loading head reached its limit. Therefore, the nanocomposite foams showed a clear change in their compressive behaviour with a marked increase in the Young's modulus. Foam theory states that the compressive modulus is directly proportional to its relative density [48]. Thus, the increase of the Young's modulus should be a combination of the density change and the reinforcement effect of the nanofiller. The Young's modulus was normalized by the relative density of the samples to eliminate the density effect (Table 3). The normalized modulus for 0.25 wt.-% FGS foam increased by over 200% and by up to 235% for 1.0 wt.-% CNT compared with the control silicone foam. In contrast, previous work on carbon nanotube/polyurethane foams [14] showed no enhancement with comparable loading fractions, and carbon nanofibre/polystyrene foams [11] showed an improvement of 136% of the normalized compressive modulus but at a considerably larger loading fraction of 5 wt.-%. The relatively large efficiency of the FGS may be attributed to favourable interactions between the FGS and the polymer. Meanwhile, the CNT case was attributed to the CNT properties and observed network.

Fig. 6 shows the experimental results for the acoustic absorption coefficient as a function of frequency. The control sample exhibited the typical behaviour of flexible open cell foams, i.e. an increase of the absorption coefficient that reached a maximum close to 1 and then a steady decrease to 0.7. This behaviour is commonly observed in open cell polyurethane foams [49]. The acoustic absorption of the filled foams varied over the entire frequency range. The absorption curves of the lowest filler loadings (0.1 wt.-% and 0.2 wt.-% FGS and 0.1 wt.-% CNTs) had a similar tendency than that of the control sample. There was, however, a reduction in the maximum and a shift of the peak to lower frequencies. Meanwhile, larger loading fractions had a

Table 3
Normalised Young's modulus and normalised sound absorption coefficient as a function of nanofiller content of the samples

Samples wt.-%	Normalised Young's modulus (MPa)	Normalised sound absorption coefficient
0	260 ± 23	0.70 ± 0.01
0.10 FGS	691 ± 28	0.56 ± 0.01
0.20 FGS	725 ± 22	0.52 ± 0.01
0.25 FGS	792 ± 27	0.45 ± 0.02
0.10 CNT	802 ± 26	0.61 ± 0.01
0.50 CNT	854 ± 28	0.47 ± 0.01
1.00 CNT	875 ± 23	0.44 ± 0.01

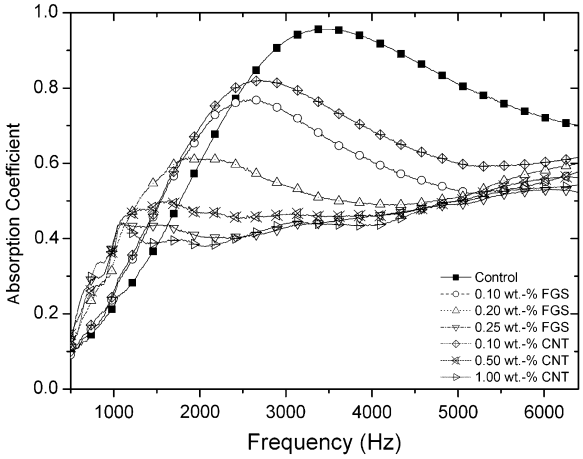

Fig. 6. Absorption coefficient as a function of frequency of the samples.

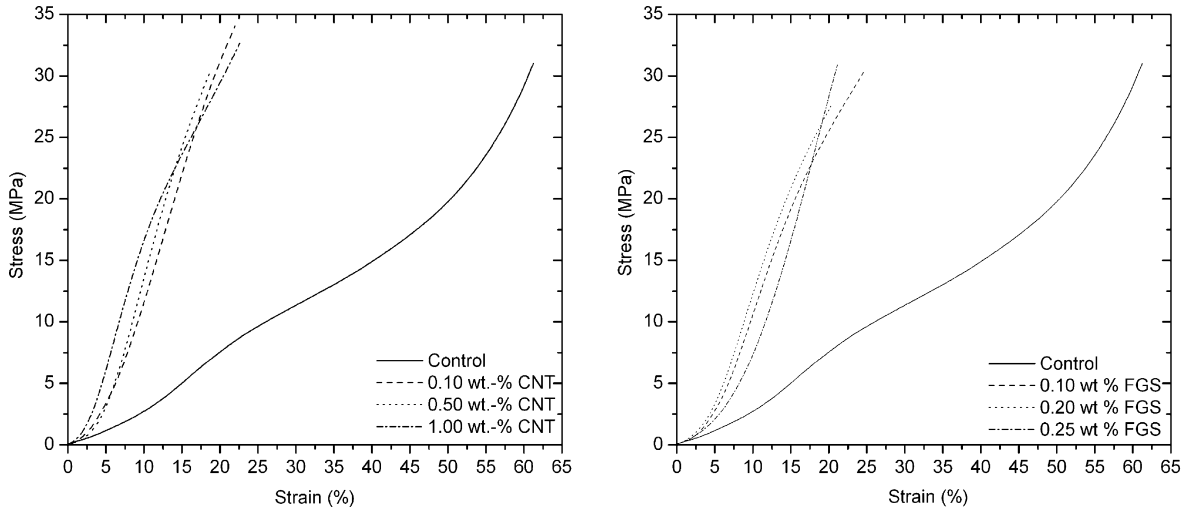

Fig. 5. Compressive stress-strain behaviour of the silicone foam nanocomposites.

drastic effect in the absorption behaviour of the samples: the absorption coefficient reached a local maximum at around 0.5 and then increased steadily to about 0.6 plus a clear shift of the peak to lower frequencies. The frequency shift and reduction of the acoustic absorption had also been observed on open cell polyolefin foams with large cell size and tortuosity [50]. The acoustic activity (Table 3), defined as the area under the absorption curve normalised by the frequency range, decreased with loading fraction regardless of the nanofiller type, with a 36% decrease for the larger loading fractions. CNT samples exhibited slightly larger values of acoustic activity than those of the FGS samples. The reason for this difference may be attributed to a different nanofiller effect on the polymer matrix because both materials showed similar cellular structure.

Therefore, the nanofillers had a negative effect on the damping properties of the foams. This result could be attributed to both the cellular structure changes and the improved mechanical properties of the cell walls and edges, as discussed below. Sound in porous materials propagates simultaneously as sound pressure waves through the fluid in the pores, and as elastic stress waves through the solid frame. Thus, sound absorption in foams is a combination of several factors: its viscoelastic and elastic properties (i.e. the material's damping and stiffness), and its viscoacoustic and acoustic properties (i.e. fluid damping controlled by fluid nature, geometry, topology, interfaces) [51]. Therefore, the acoustic behaviour of foams is a complex mechanism where several factors have to be considered. A common approach to improve sound absorption in porous materials is to reduce the cell size, which is usually accompanied by an increase in the tortuosity [52]. In our case, even though we had a reduction of the cells connectivity (or an increase in the tortuosity), we observed an opposite tendency. This trend may be related to a reduction of the dissipation of acoustic energy by vibration damping due to larger cells sizes (there were less number of pores for the sound to be absorbed) and improved modulus (filled samples had stiffer cell edges and faces). Furthermore, the suggested strong interface of FGS and CNT to the polymer matrix may also account for the reduced damping properties as damping effects of CNTs within polymers were attributed to high frictional energy dissipation due to interfacial sliding and stick-slip behaviour of CNT surfaces [53].

Conclusions

The present work presents the physical properties of nanocomposite silicone foams filled with two different carbon-based nanofillers, functionalized graphene sheets and nanotubes. The nanofillers had a similar effect on the cellular structure, yielding larger cell size than pristine foam. The thermal stability of the samples was drastically affected by the presence of both nanofillers, with an increase of the degradation temperature of more than 50 °C. FGS however showed a greater improvement attributed to an increased confinement of the polymer matrix in the intercalated structure and improved polymer/graphene interactions.

Both nanofillers had a positive effect on the mechanical properties of the nanocomposite samples. The CNT sample outperforms the FGS with similar loading content due to the CNT properties and the network formation. Meanwhile, the nanofillers had a negative effect on the sound absorption capabilities. This result was attributed to two possible mechanisms, the changes in the cellular morphology and mechanical properties of the foams and the strong interface of FGS and CNT with the polymer matrix. The strong interface thought to be most suitable for straightforward reinforcement [1] may be less desirable for damping applications.

Further research is required to better understand the effect of the nanofillers on the foaming mechanism and rheology, and to minimise their effect on the cellular structure.

Acknowledgements

The authors of this study gratefully acknowledge the financial support of Consejo Superior de Investigaciones Cientificas (CSIC) – Comunidad de Madrid (Spain) through its project CCG07-CSIC/MAT-2336. R. Verdejo also acknowledges a Juan de la Cierva contract from the Spanish Ministry of Science (MEC).

References

[1] Coleman JN, Khan U, Gun'ko YK. Mechanical reinforcement of polymers using carbon nanotubes. Adv Mater 2006;18(6):689–706.
[2] Shaffer MS, Sandler J. In: Advani S, editor. Carbon nanotube/nanofibre polymer composites. World Scientifc; 2006. p. 1–59.
[3] Cadek M, Coleman JN, Ryan KP, Nicolosi V, Bister G, Fonseca A, et al. Reinforcement of polymers with carbon nanotubes: the role of nanotube surface area. Nano Lett 2004;4(2):353–6.
[4] Lahiff E, Ryu CY, Curran S, Minett AI, Blau WJ, Ajayan PM. Selective positioning and density control of nanotubes within a polymer thin film. Nano Lett 2003;3(10):1333–7.
[5] Olek M, Ostrander J, Jurga S, Mohwald H, Kotov N, Kempa K, et al. Layer-by-layer assembled composites from multiwall carbon nanotubes with different morphologies. Nano Lett 2004;4(10):1889–95.
[6] Raravikar NK. Synthesis and characterization of thickness-aligned carbon nanotube-polymer composite films. Chem Mater 2005;17(5):974–83.
[7] Valentini L, Biagiotti J, López-Manchado MA, Santucci S, Kenny JM. Effects of carbon nanotubes on the crystallization behavior of polypropylene. Polym Eng Sci 2004;44(2):303–11.
[8] Liu T, Kumar S. Effect of orientation on the modulus of SWNT films and fibers. Nano Lett 2003;3(5):647–50.
[9] Gao J, Itkis ME, Yu A, Bekyarova E, Zhao B, Haddon RC. Continuous spinning of a single-walled carbon nanotube-nylon composite fiber. J Am Chem Soc 2005;127(11):3847–54.
[10] Sandler JKW, Pegel S, Cadek M, Gojny F, van Es M, Lohmar J, et al. A comparative study of melt spun polyamide-12 fibres reinforced with carbon nanotubes and nanofibres. Polymer 2004;45(6):2001–15.
[11] Lee LJ, Zeng C, Cao X, Han X, Shen J, Xu G. Polymer nanocomposite foams. Compos Sci Technol 2005;65(15–16):2344–63.
[12] Jell G, Verdejo R, Safinia L, Stevens M, Shaffer M, Bismarck A. Carbon nanotube enhanced polyurethane scaffolds fabricated by thermally induced phase separation. J Mater Chem 2008;18:1865–72.
[13] Park K-Y, Lee S-E, Kim C-G, Han J-H. Fabrication and electromagnetic characteristics of electromagnetic wave absorbing sandwich structures. Compos Sci Technol 2006;66(3-4):576–84.
[14] Verdejo R, Jell G, Safinia L, Bismarck A, Stevens M, Shaffer M. Reactive polyurethane carbon nanotube foams and their interactions with osteoblasts. J Biomed Mater Res A 2008 [accepted for publication]. doi: 10.1002/jbm.a.31698.
[15] Werner P, Verdejo R, Wöllecke F, Altstädt V, Sandler JKW, Shaffer MSP. Carbon nanofibers allow foaming of semicrystalline poly(ether ether ketone). Adv Mater 2005;17(23):2864–9.

[16] Yang Y, Gupta MC, Dudley KL, Lawrence RW. Conductive carbon nanofiber-polymer foam structures. Adv Mater 2005;17(16): 1999–2003.
[17] Yang Y, Gupta MC, Dudley KL, Lawrence RW. Novel carbon nanotube-polystyrene foam composites for electromagnetic interference shielding. Nano Lett 2005;5(11):2131–4.
[18] McAllister MJ, Li JL, Adamson DH, Schniepp HC, Abdala AA, Liu J, et al. Single sheet functionalized graphene by oxidation and thermal expansion of graphite. Chem Mater 2007;19(18):4396–404.
[19] Schniepp HC, Li JL, McAllister MJ, Sai H, Herrera-Alonso M, Adamson DH, et al. Functionalized single graphene sheets derived from splitting graphite oxide. J Phys Chem B 2006;110(17):8535–9.
[20] Stankovich S, Dikin DA, Piner RD, Kohlhaas KA, Kleinhammes A, Jia Y, et al. Synthesis of graphene-based nanosheets via chemical reduction of exfoliated graphite oxide. Carbon 2007;45(7):1558–65.
[21] Dresselhaus MS, Dresselhaus G. Intercalation compounds of graphite. Adv Phys 2002;51(1):1–186.
[22] Chen G, Weng W, Wu D, Wu C. PMMA/graphite nanosheets composite and its conducting properties. Eur Polym J 2003;39:2329.
[23] Chen G, Wu D, Weng W, Wu C. Exfoliation of graphite flake and its nanocomposites. Carbon 2003;41(3):619–21.
[24] Chen GH, Chen XF, Wang HQ, Wu DJ. Dispersion of graphite nanosheets in polymer resins via masterbatch technique. J Appl Polym Sci 2007;103(6):3470–5.
[25] Chen GH, Weng WG, Wu DJ, Wu CL, Lu JR, Wang PP, et al. Preparation and characterization of graphite nanosheets from ultrasonic powdering technique. Carbon 2004;42(4):753–9.
[26] Ramanathan T, Stankovich S, Dikin DA, Liu H, Shen H, Nguyen ST, et al. Graphitic nanofillers in PMMA nanocomposites – an investigation of particle size influence on nanocomposite and dispersion and their properties. J Polym Sci B: Polym Phys 2007;45(15):2097–112.
[27] Uhl FM, Wilkie CA. Polystyrene/graphite nanocomposites: effect on thermal stability. Polym Degrad Stab 2002;76(1):111–22.
[28] Weng WG, Chen GH, Wu DJ, Chen XF, Lu JR, Wang PP. Fabrication and characterization of nylon 6/foliated graphite electrically conducting nanocomposite. J Polym Sci B: Polym Phys 2004;42(15):2844–56.
[29] Stankovich S, Dikin DA, Dommett GHB, Kohlhaas KM, Zimney EJ, Stach EA, et al. Graphene-based composite materials. Nature 2006;442(7100):282–6.
[30] Verdejo R, Barroso-Bujans F, Rodriguez-Perez MA, de Saja JA, López-Manchado MA. Functionalized graphene sheet filled silicone foams. J Mater Chem 2008;18:2221–6.
[31] Kim H, Macosko CW. Morphology and properties of polyester/exfoliated graphite nanocomposites. Macromolecules 2008;41(9):3317–27.
[32] Klempner D, Frisch KC. Handbook of polymeric foams and foam technology. Hanser Publishers; 1991.
[33] Harper JR, Baumann Menko TM, Nicholson W. Silicone foams. In: Klempner D, Sendijarevic V, editors. Munich, Germany: Hanser Publishers; 2004. p. 379–89.
[34] Brodie BC. On the atomic weight of graphite. Philos Trans R Soc (1776–1886) 1859;149(-1):249–59.
[35] Saunders JH, Klempner D. Fundamentals of foam formation. Hanser Publishers; 2004.
[36] Lee YH, Wang KH, Park CB, Sain M. Effects of clay dispersion on the foam morphology of LDPE/clay nanocomposites. J Appl Polym Sci 2007;103(4):2129–34.
[37] Shen J, Zeng C, Lee LJ. Synthesis of polystyrene-carbon nanofibers nanocomposite foams. Polymer 2005;46(14):5218–24.
[38] Everitt SL, Harlen OG, Wilson HJ, Read DJ. Bubble dynamics in viscoelastic fluids with application to reacting and non-reacting polymer foams. J Non-Newtonian Fluid Mech 2003;114:83–107.
[39] Shaffer MSP, Windle AH. Analogies between polymer solutions and carbon nanotube dispersions. Macromolecules 1999;32(20): 6864–6.
[40] Knauert ST, Douglas JF, Starr FW. The effect of nanoparticle shape on polymer-nanocomposite rheology and tensile strength. J Polym Sci B-Polym Phys 2007;45(14):1882–97.
[41] Giannelis EP. Polymer layered silicate nanocomposites. Adv Mater 1996;8(1):29–35.
[42] Suezawa H, Yoshida T, Ishihara S, Umezawa Y, Nishio M. CH/p interactions as disclosed on the fullerene convex surface. A database study. Cryst Eng Comm 2003;5(93):514–8.
[43] Nishio M, Hirota M, Umezawa Y. The CH/p interaction. Evidence, nature, and consequences. New York: Wiley-VCH; 1998.
[44] Camino G, Lomakin SM, Lageard M. Thermal polydimethylsiloxane degradation. Part 2. The degradation mechanisms. Polymer 2002;43(7):2011–5.
[45] Moniruzzaman M, Winey KI. Polymer nanocomposites containing carbon nanotubes. Macromolecules 2006;39(16):5194–205.
[46] Zhang J, Feng S, Ma Q. Kinetics of the thermal degradation and thermal stability of conductive silicone rubber filled with conductive carbon black. J Appl Polym Sci 2003;89:1548–54.
[47] Burnside SD, Giannelis EP. Synthesis and properties of new poly(dimethylsiloxane) nanocomposites. Chem Mater 1995;7(9):1597–600.
[48] Gibson LJ, Ashby MF. Cellular solids: structure and properties. Cambridge University Press; 1997.
[49] Laurikis W. Acoustic characteristics of low density foams. In: Hilyard NC, C A, editors. London: Chapman and Hall; 1994 [Chapter 10].
[50] Alvarez-Lainez M, Rodriguez-Perez MA, de Saja JA. Microstructure and physical properties of open-cell polyolefin foams. J Appl Polym Sci [accepted for publication].
[51] Göransson P. Tailored acoustic and vibrational damping in porous solids – engineering performance in aerospace applications. Aerosp Sci Technol 2008;12:26–41.
[52] Allard JF. Propagation of sound in porous media: modelling sound absorbing materials. Elsevier Applied Science 1993.
[53] Suhr J, Koratkar N, Keblinski P, Ajayan PM. Viscoelasticity in carbon nanotube composites. Nat Mater 2005;4:134–7.